Int. J. Electrochem. Sci., 14 **(2019)** 8382 – 8392, doi: 10.20964/2019.09.35

International Journal of
ELECTROCHEMICAL
SCIENCE
www.electrochemsci.org

Phase Structure and Electrochemical Performances of $La_{0.63}Gd_{0.2}Mg_{0.17}Ni_{3.0-x}Co_{0.3}Al_x$ (x = 0.0, 0.1, 0.2, 0.3, 0.4) Alloys

Zhijie Gao [1,*], *Yongchun Luo* [2,*]

[1] Department of Chemical Engineering and Safety, Binzhou University, Binzhou 256600, PR China
[2] School of Materials Science and Engineering, Lanzhou University of Technology, Lanzhou 730050, PR China
[*]E-mail: gaozhijie1983@126.com, luoyc@lut.cn

Received: 5 April 2019 / *Accepted:* 27 June 2019 / *Published:* 31 July 2019

The influences of Al substitution for Ni on the phase abundance, structures and electrochemical properties of $La_{0.63}Gd_{0.2}Mg_{0.17}Ni_{3.0-x}Co_{0.3}Al_x$ (x = 0.0, 0.1, 0.2, 0.3, 0.4) alloys have been investigated. The main phase of Al-free base alloy is Ce_2Ni_7-type phase, Gd_2Co_7-type phase and $CeNi_3$-type phase. After a little Al substitution, AB_3 phase shifts to A_2B_7 phase. Further Al addition promotes the formation of $CaCu_5$-type phase over the A_2B_7-type phase. The sample of x = 0.1 (AB_3 to A_2B_7) increases cycling stability and its discharge capacity almost unchanged. The further addition of Al (A_2B_7 to $CaCu_5$) still increases cycling stability, but decreases the maximum discharge capacity and high rate dischargeability. The substitution of Al elements increases the phase abundance of A_2B_7-type or $CaCu_5$-type so as to improve the cycling stability. The ability of phase pulverization resistance of the metal hydride alloy at the negative electrode appeared to be the intrinsic reason of failure mode of this series of alloys.

Keywords: La-Mg-Ni-based hydrogen storage alloy, Al substitution, Microstructure, Electrochemical properties

1. INTRODUCTION

La-Mg-Ni system hydrogen storage alloys are determined as a new generation anode materials of nickel/metal hydride batteries because of their high discharge capacity (~410 mAh g^{-1}) [1, 2], superior high rate dischargeability [3], environmental friendliness [4] and other advantages [5-12]. However, their cycle life need to be further improved to satisfy the urgent demand for a power source with favorable overall electrochemical performance.

It is well known that a large number of investigations on La-Mg-Ni-based alloy have been carried out [13-18]. The research on the inferior cycling stability of their alloys is still further understanding. Although the intrinsic reason for the inferior cycling stability of the alloy is not clear,

the previous research has accumulated a lot of valuable information. Some important enlightenments have also been drawn as follows:

(1) At present, most of the annealed La-Mg-Ni-based alloys in the study form multiphase structures, resulting in uneven distribution of alloy composition. The above mentioned greatly affects the study of the mechanism of action of rare earth elements, and it has also been difficult to make a correct analysis and evaluation of the electrochemical behavior and performance of single phase. (2) The atomic size of rare earth elements affects the phase transformation, structural stability and hydrogen induced amorphization (HIA) tendency of the alloys. The order of the atomic radii of rare earth elements is $r_{La} > r_{Pr} > r_{Ce} > r_{Nd} > r_{Sm} > r_{Gd}$ [11, 19-23]. Based on $r_A / r_B > 1.37$ (r_A and r_B stand for the atomic radii of the A and B elements of the AB_n alloy, respectively) [20], it may have a profound effect on HIA and electrochemical properties of Ce_2Ni_7-type alloys by making use of partial replacement of La with rare earth elements with a smaller atomic radii. (3) B-side elements with larger atomic radii such as Co and Al may affect the phase structural stability and reduce or avoid the tendency of HIA, resulting in profound effect of electrochemical behavior and performance.

In addition, Young et al. [24] reported partial substitution of Al for Co in the $La_{0.7}Mg_{0.3}Ni_{2.8}Co_{0.5-x}Al_x$ (x = 0-0.2) alloys and found that the main phase shifted from A_2B_7 into AB_5 with Al. The hydrogen storage capacity, pressure, and hysteresis in the gas phase decreased with Al. The storage capacity, high rate dischargeability and low temperature performance of the battery deteriorated with Al. It can clearly be seen that charge retention and cycling stability of the alloy improved with Al. Al elements render tremendous influence in the cycling stability of La-Mg-Ni-based $AB_{3.3}$-type alloys. Therefore, the substitution method of Al elements is supposed to be promising on $AB_{3.3}$-type alloys. Furthermore, by adjusting the content of low Mg and rich-lanthanum rare earth elements combined with Al, it may be an important way to further improve the cycling stability of Ce_2Ni_7-type alloy electrode, but this has hardly been reported so far.

Based on the discussion above, in this study, Al are used to partially substitute for Ni in $La_{0.63}Gd_{0.2}Mg_{0.17}Ni_{3.0-x}Co_{0.3}Al_x$ (x = 0.0, 0.1, 0.2, 0.3, 0.4) alloys. The effects of the Al-substitution on the phase evolution and electrochemical performances of the alloys are investigated. The synergistic effects of Al and Gd have been illustrated. It is expected that a proper amount of Al substitution for Ni can effectively ameliorate the overall electrochemical performances, especially the cycling stability of the La-Mg-Ni-based alloys.

2. EXPERIMENTAL DETAILS

2.1 Sample Preparation

The alloys designed as $La_{0.63}Gd_{0.2}Mg_{0.17}Ni_{3.0-x}Co_{0.3}Al_x$ (x = 0.0, 0.1, 0.2, 0.3, 0.4) were prepared by the induction melting method at 0.4 MPa of Ar atmosphere. The ingots were annealed for 8 hours at 1173 K under Ar pressure (0.1 MPa). A compensation of 5 wt.% of both rare earth elements and Mg was applied due to the burning loss. The purity of all elements was above 99.9 wt.%.

2.2 Structural and Electrochemical Characterization

The annealed alloy was mechanically pulverized into powder (<38 μm) for X-ray diffraction (XRD) measurement, and 400 mesh powder was used for electrochemical tests. XRD tests were measured on a Rigaku D / max-2400 diffractometer. Its power is 40 kV x 150 mA with Cu radiation. The pattern was recorded in the range of 15° to 90° in which the step size of 2θ was 0.02°. Then the collected data were analyzed by the Rietveld method [25] using Fullprof 2000 software [26] to get the lattice parameters. The backscattered electron images were obtained by making use of Electron probe micro analyzer (EPMA-1600) with wave dispersive spectroscopy (WDS), which was used to characterize the phase structure and the composition of alloys.

The annealed alloy powders of ~0.1g were selected from 54 to 61 microns and the electrodes were prepared. The alloy electrode was synthesized by cold pressing under 20 MPa pressure. It consists of a mixture, which contains the alloy powder and nickel carbonyl powder at a weight ratio of 1:3, then forms anodes with a diameter of 10 mm. The electrochemical tests were carried out in a standard open three-electrode system at 298K. The cell consists of an alloy electrode, a sintered $Ni(OH)_2$/NiOH cathode, a Hg/HgO reference electrode, 6M KOH electrolyte and a diaphragm. Each alloy electrode is discharged to the cut-off potential -0.6 V vs. Hg/HgO reference electrode. During the activation process, the electrode was charged/discharged at a current density of 60 mA g^{-1}. When the cycle stability at 298 K was checked, the electrode was charged/discharged at a current density of 300 mA g^{-1}.

3. RESULTS AND DISCUSSION

3.1 Alloy crystal structure

Fig. 1 shows the XRD patterns for $La_{0.63}Gd_{0.2}Mg_{0.17}Ni_{3.0-x}Co_{0.3}Al_x$ (x = 0.0, 0.1, 0.2, 0.3, 0.4) alloys. According to the Rietveld refinement analyses, the abundance of phase was tabulated in Table 1. Rietveld analysis of x = 0.1 alloys is shown in Figure 2. It can be seen that all of alloys are multi-phase structures. The phase structures include the Ce_2Ni_7-type (Gd_2Co_7-type) phase, the $CeNi_3$-type phase and $CaCu_5$-type phase. From Table 1, it can be seen that the addition of Al has significant effect on the alloy phase structures. The phase abundance of the Ce_2Ni_7-type (Gd_2Co_7-type) structure of these alloys firstly increases then decreases as Al increases. The $CeNi_3$-type phase and $CaCu_5$-type phase gradually decrease and increase, respectively. Compared to the Al-free alloy, the phase abundance of Ce_2Ni_7-type (Gd_2Co_7-type) structure of x = 0.1 alloy slightly increases to 71.94 wt.%, $CeNi_3$-type structure decreases to 19.67 wt.% and the $CaCu_5$-type phase appears. Moreover, the further addition of Al promotes Ce_2Ni_7-type (Gd_2Co_7-type) to change to $CaCu_5$-type phase. When the stoichiometric ratio of Al element is > 0.1, the Ce_2Ni_7-type (Gd_2Co_7-type) phase structure significantly decreases, and the $CaCu_5$-type phase also significantly increases. This is consistent with the reports in references [9] and [24].

The cell parameters of all phases for each sample are listed in Table 2. After substitution, both a and c cell parameters in the Ce_2Ni_7-type structure of alloys slightly increase, and the unit cell of the $CaCu_5$-type phase stretches longer along c-axis. The c/a ratio is 0.7952, 0.7971, 0.8017 and 0.8031,

respectively. Increases in the c/a ratio in $CaCu_5$-type phase is related to lower rates of pulverization during hydrogenation/dehydrogenation cycle [27]. Here, the pulverization rate decreases as Al increases while the c/a ratio increases.

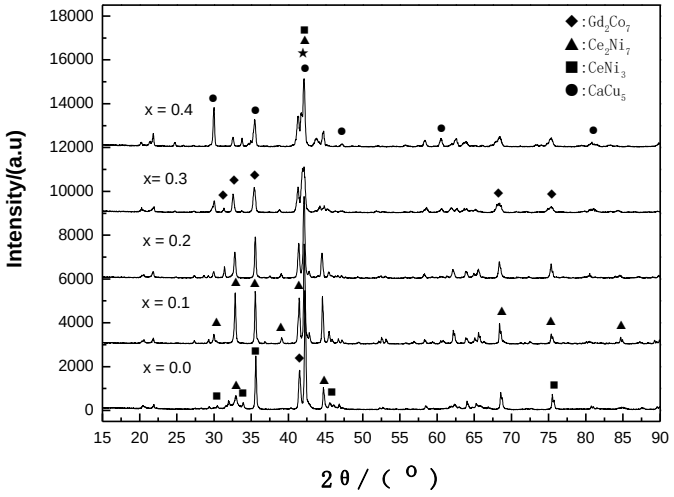

Figure 1. XRD patterns for $La_{0.63}Gd_{0.2}Mg_{0.17}Ni_{3.0-x}Co_{0.3}Al_x$ (x = 0.0, 0.1, 0.2, 0.3, 0.4) alloys

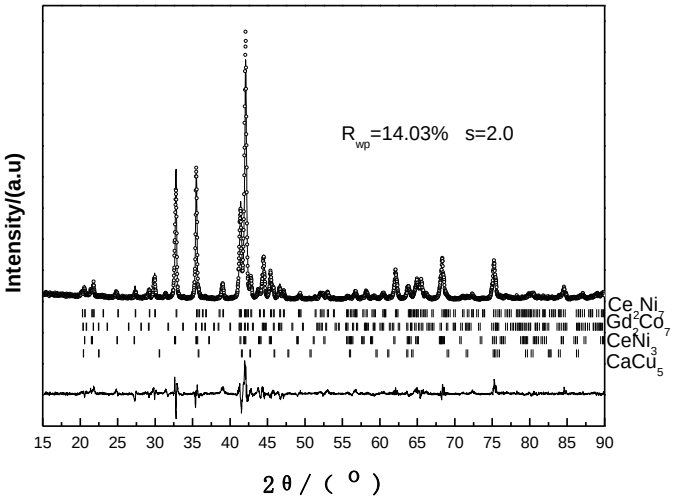

Figure 2. Rietveld refinement of the XRD patterns for $La_{0.63}Gd_{0.2}Mg_{0.17}Ni_{2.9}Co_{0.3}Al_{0.1}$ alloys.

Table 1. Phase abundance (wt%) calculated from XRD analysis for $La_{0.63}Gd_{0.2}Mg_{0.17}Ni_{3.0-x}Co_{0.3}Al_x$ (x = 0.0, 0.1, 0.2, 0.3, 0.4) alloys

	Ce_2Ni_7	Gd_2Co_7	$CeNi_3$	$CaCu_5$
x = 0.0	40.80	28.72	30.48	0.00
x = 0.1	66.97	4,97	19.67	8.39
x = 0.2	51.53	5.67	8.08	34.72
x = 0.3	35.34	8.79	6.11	49.76
x = 0.4	16.78	7.58	5.99	69.65

Table 2. Lattice constants of $La_{0.63}Gd_{0.2}Mg_{0.17}Ni_{3.0-x}Co_{0.3}Al_x$ (x = 0.0, 0.1, 0.2, 0.3, 0.4) alloys from XRD analysis

	Ce_2Ni_7		Gd_2Co_7		$CeNi_3$		$CaCu_5$	
	a (nm)	c (nm)	a (nm)	c (nm)	a (nm)	c (nm)	a (nm)	c (nm)
x = 0.0	0.5032	2.4254	0.5031	3.6443	0.5009	2.4863	-	-
x = 0.1	0.5040	2.4345	0.5041	3.6656	0.5019	2.4737	0.5015	0.3988
x = 0.2	0.5046	2.4379	0.5043	3.6594	0.5037	2.4622	0.5032	0.4011
x = 0.3	0.5051	2.4484	0.5040	3.6935	0.5071	2.4613	0.5039	0.4040
x = 0.4	0.5052	2.4549	0.5033	3.7195	0.5078	2.4497	0.5044	0.4051

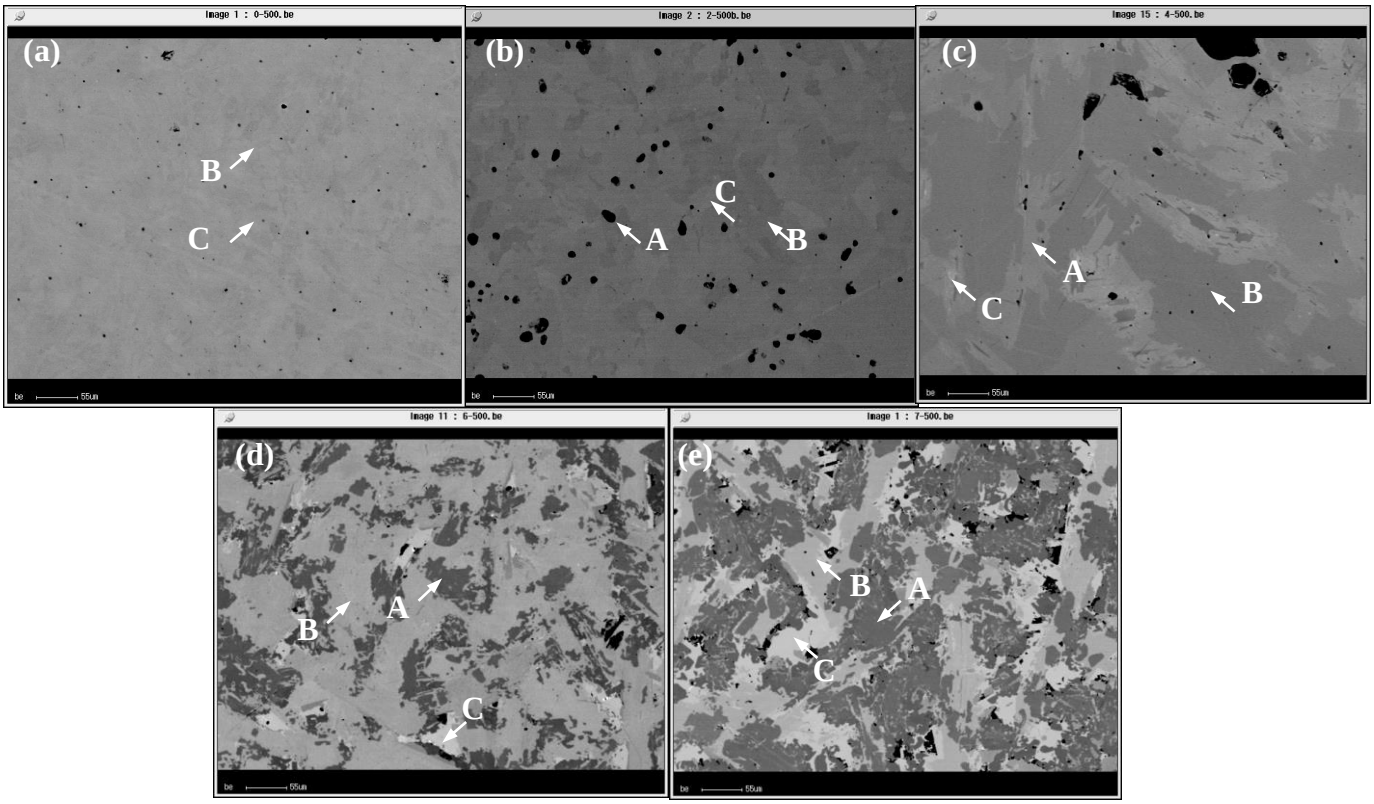

Figure 3. Back scattered electron images for $La_{0.63}Gd_{0.2}Mg_{0.17}Ni_{3.0-x}Co_{0.3}Al_x$: (a) x = 0.0, (b) x = 0.1, (c) x = 0.2, (d) x = 0.3 and (e) x = 0.4 (A: $CaCu_5$-type phase, B: Ce_2Ni_7-type (Gd_2Co_7-type) phase, C: $CeNi_3$-type phase)

Fig. 3 presents the back scattering electron images of $La_{0.63}Gd_{0.2}Mg_{0.17}Ni_{3.0-x}Co_{0.3}Al_x$ (x = 0.0, 0.1, 0.2, 0.3, 0.4). There are two areas of x = 0.0 and three areas of x = 0.1~0.4 in the image which are black, dark grey and light grey, respectively. Combining with WDS analysis and Rietveld analysis, the black area (A area) can be identified as $CaCu_5$-type phase, the dark grey regions (B area) can be identified as Ce_2Ni_7-type (Gd_2Co_7-type) $(RE,Mg)_2Ni_7$ phase, the light grey area (C area) can be identified as $CeNi_3$-type phase. This is also consistent with the XRD results.

3.2 Charge/discharge characteristics

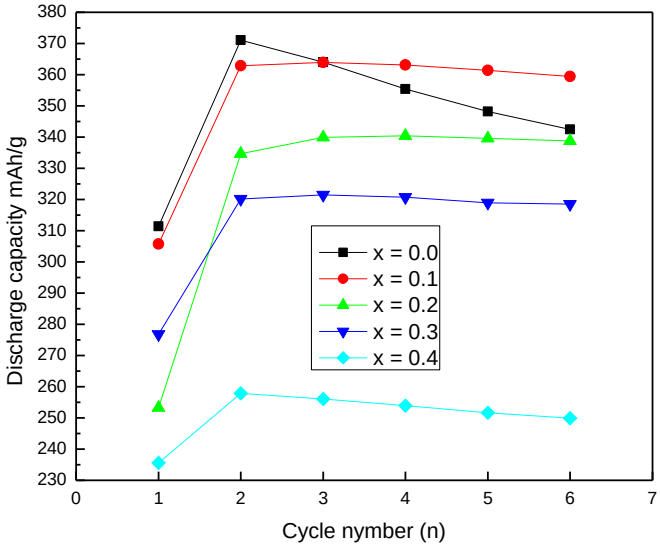

Figure 4. Activation curves of $La_{0.63}Gd_{0.2}Mg_{0.17}Ni_{3.0-x}Co_{0.3}Al_x$ (x = 0.0, 0.1, 0.2, 0.3, 0.4) annealed alloy electrodes with 60 mA g^{-1} charge-discharge current density at 298 K

Table 3. Summary of electrochemical performance for $La_{0.63}Gd_{0.2}Mg_{0.17}Ni_{3.0-x}Co_{0.3}Al_x$ (x = 0.0, 0.1, 0.2, 0.3, 0.4) annealed alloy electrodes at 298 K

Sample	N	C_{max} (mAh g^{-1})		S_{100} (%)	HRD_{900} (%)	I_0 (mA g^{-1})
		60 mA g^{-1}	300 mA g^{-1}			
x = 0.0	2	371.1	335.1	76.2	75.2	218.5
x = 0.1	3	363.9	327.8	90.4	72.0	201.6
x = 0.2	4	340.4	308.0	90.6	70.0	193.5
x = 0.3	3	321.5	296,0	92,6	66.0	175.5
x = 0.4	2	257.9	228.3	91.8	61.4	168.3

The activation curve of the alloy electrodes at 298K is shown in Fig. 4. Table 3 lists the electrochemical performance parameters of the alloy electrodes at 298K. It can be found that Al element substitution has little effect on the activation rates of the alloy electrodes. All of alloy electrodes exhibit good activation characteristics after 2 to 4 charge/discharge cycles. However, the effect of Al element significantly reduces the discharge capacity of the alloy electrode. Depending on the amount of Al substitution, the discharge capacity is 363.9, 340.4, 321.5 and 257.9 mAh g^{-1}, respectively. These results are lower than the Al-free alloy. This is largely due to the shift of the main phase from Ce_2Ni_7-type (Gd_2Co_7-type) structure to $CaCu_5$-type phase, i.e. from higher capacity to lower capacity. This result is different from the results obtained in AB_2 [28] and AB_5 [29] alloy electrodes, but consistent with La-Mg-Ni-based AB_3-type alloy [24].

3.3 Cycling stability

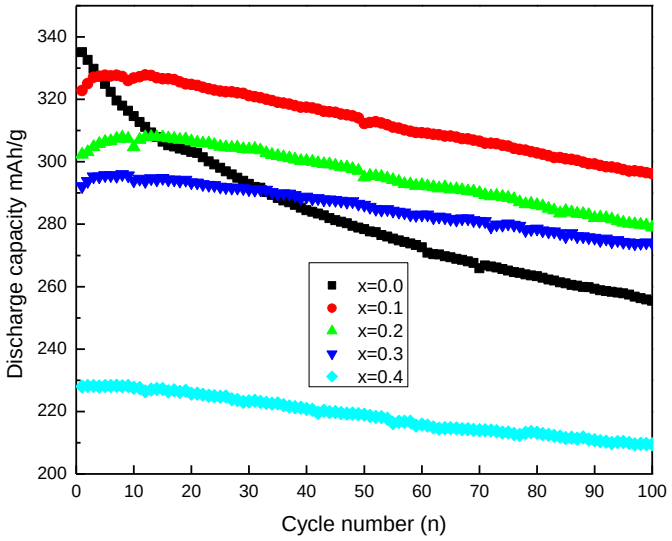

Figure 5. The cycling stability of $La_{0.63}Gd_{0.2}Mg_{0.17}Ni_{3.0-x}Co_{0.3}Al_x$ (x = 0.0, 0.1, 0.2, 0.3, 0.4) annealed alloy electrodes at 298K

The $La_{0.63}Gd_{0.2}Mg_{0.17}Ni_{3.0-x}Co_{0.3}Al_x$ (x = 0.0, 0.1, 0.2, 0.3, 0.4) alloy electrodes are subjected to 100 charge/discharge cycles. The discharge capacity retention curves are presented in Fig. 5. The cycling stability of alloy electrodes is evaluated by making use of capacity retention rate after 100 charge/discharge cycles. The capacity retention at the 100^{th} cycle (S_{100}) is defined as the ratio of $C_{100}/C_{max} \times 100\%$ (where C_{max} is the maximum discharge capacity and is C_{100} the discharge capacity at the 100^{th} cycles [19]), and is listed in Table 3. It can be found that the S_{100} of all alloy electrodes varied between 92.6% and 76.2%. Compared to the Al-free alloy, the cycling stability of alloy electrodes has been improved as expected. From the results it is indicated that the role of Al elements in AB_3-type alloy is similar with that in AB_5-type alloy [29]. So, the improvement should not only result from the refinement of the alloy surface, but also be due to the change of the pulverization rate of alloys. It is well known that pulverization is a fundamental reason for the capacity decay of the electrode alloys. Pulverization further causes severe oxidation. The anti-pulverization capability of the alloys basically depends on their grain size [30]. The order of c/a ratio of alloys is x = 0.4 > x = 0.3 > x = 0.2 > x = 0.1 and it is known that partial substituting Ni with Al elements can reduce the pulverization [31, 32]. The Al element should make contribution to the anti-pulverization.

3.4 Electrochemical kinetic characteristics

The high rate dischargeability (HRD) was measured at various discharge current densities of 300 mA g^{-1}, 600 mA g^{-1} and 900 mA g^{-1} on CHI660a electrochemical work station. The HRD can be defined as follows:

$$HRD = (C_d/C_{60}) \times 100\% \quad (1)$$

where C_d is the discharge capacity at the various discharge current densities of 300 mA g^{-1}, 600 mA g^{-1} and 900 mA g^{-1} with the cutoff of -0.6 V VS Hg/HgO reference electrode, C_{60} is the maximum discharge capacity during activation. Fig. 6(a) shows the HRD curves of the alloy electrodes at various current densities. Table 3 lists the values of the HRD_{900} at a current density of 900 mA g^{-1}. It can be found that the high rate dischargeability is obviously deteriorated by the partial Al substitution. The HRD_{900} decreased from 75.2% to 61.4% as x increases from 0 to 0.4. Furthermore, we found that the x = 0.4 alloy with the highest abundance of AB_5-type phase may have lowest HRD compared to Ce_2Ni_7-type phase. This is consistent with the reports in references [24].

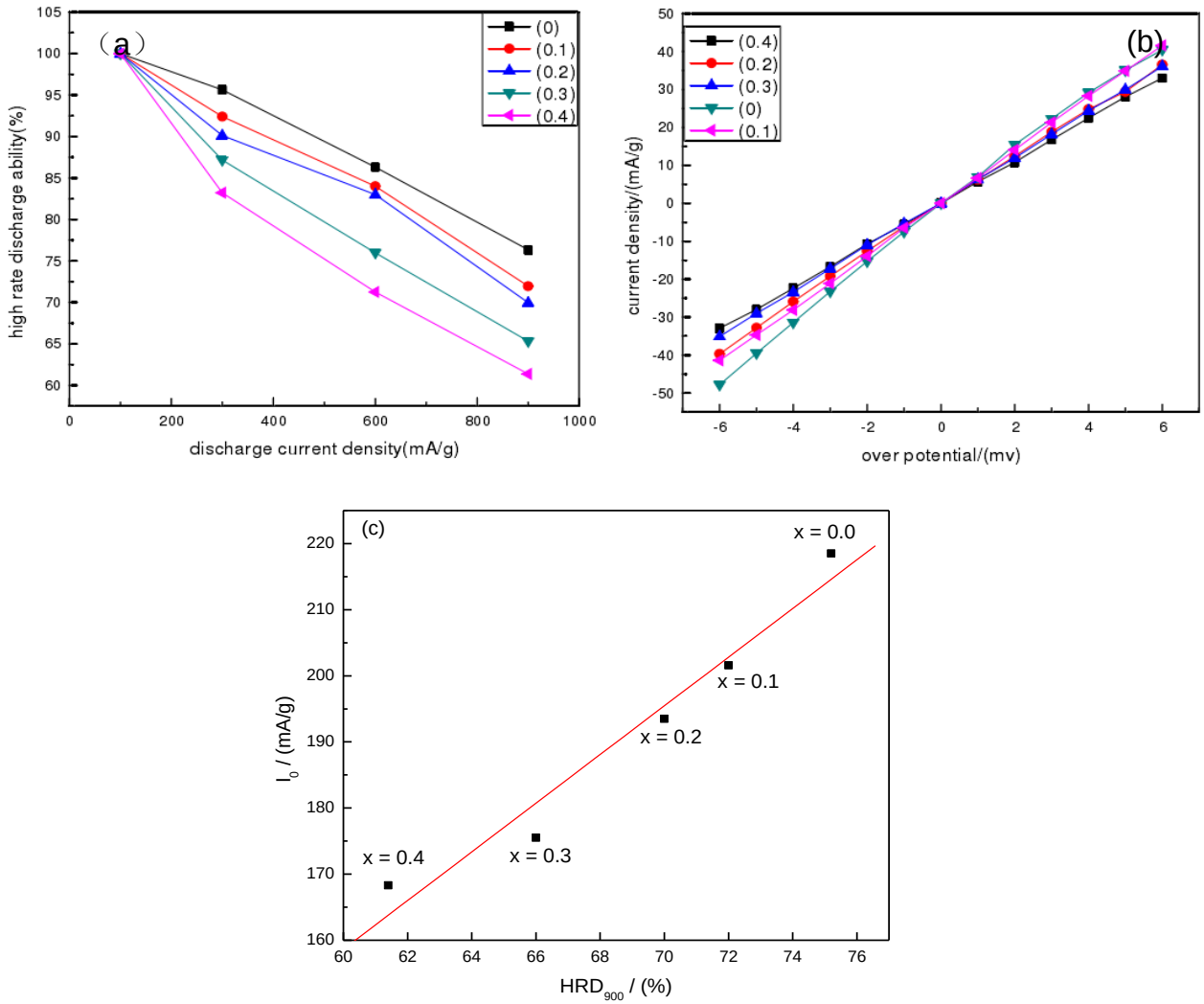

Figure 6. HRD of the $La_{0.63}Gd_{0.2}Mg_{0.17}Ni_{3.0-x}Co_{0.3}Al_x$ alloy at various discharge current densities (a), Linear polarization curves of the alloys (b), and relationship between HRD_{900} and I_0 of the alloys (c)

The HRD of the nickel-metal hydride batteries is determined by the kinetic properties of hydrogenation/dehydrogenation reactions [33]. The kinetic properties are basically controlled with the diffusion of hydrogen atoms in the bulk phase of the alloys and the charge transfer rate of alloy surface.

They are characterized by hydrogen diffusion coefficient (D_0) and exchange current density (I_0), respectively [34]. Fig.6 (b) shows the linear polarization curves of the $La_{0.63}Gd_{0.2}Mg_{0.17}Ni_{3.0-x}Co_{0.3}Al_x$ alloys. According to the slope of linear polarization curve, I_0 can be calculated as follows:

$$I_0 = RTI_d / (F\eta) \quad (2)$$

where R is the gas constant, T is the absolute temperature, I_d is the applied current density, F is the Faraday constant and η is the total overpotential. The I_0 is summarized in Table 3. It can be found that I_0 decreases from 218.5 mA g^{-1} to 168.3 mA g^{-1} as x increase. Iwakura et al. [35] pointed out that if the electrochemical reaction on the alloy surface was rate-determining, a linear dependence of HRD on the exchange current density could be observed, while if the hydrogen diffusion in the alloy bulk was rate-determining, the HRD would be constant irrespective of exchange current density. The relationship between the HRD_{900} and the I_0 is shown in Fig. 6 (c). It can be observed that the dependence of the HRD_{900} on the I_0 is linearly fitted well and the error is calculated to be 0.0211, which is within the allowed error range.

The electrochemical properties including C_{max} and S_{100} of $AB_{3.3}$-type $La_{0.63}Gd_{0.2}Mg_{0.17}Ni_{3.0-x}Co_{0.3}Al_x$ alloys, $La_{0.7}Mg_{0.3}Ni_{2.8}Co_{0.5-x}Al_x$ (x = 0-0.2) alloys [24] and $Mm_{0.83}Mg_{0.17}Ni_{3.1}Al_{0.2}$ alloy [31] are presented in Table 4. The C_{max} and S_{100} are in the order of: $La_{0.63}Gd_{0.2}Mg_{0.17}Ni_{2.9}Co_{0.3}Al_{0.1}$ alloy ~ $La_{0.7}Mg_{0.3}Ni_{2.8}Co_{0.4}Al_{0.1}$ alloy > $Mm_{0.83}Mg_{0.17}Ni_{3.1}Al_{0.2}$ alloy and $Mm_{0.83}Mg_{0.17}Ni_{3.1}Al_{0.2}$ alloy > $La_{0.63}Gd_{0.2}Mg_{0.17}Ni_{2.9}Co_{0.3}Al_{0.1}$ alloy > $La_{0.7}Mg_{0.3}Ni_{2.8}Co_{0.4}Al_{0.1}$ alloy, respectively. The overall electrochemical performance of $La_{0.63}Gd_{0.2}Mg_{0.17}Ni_{2.9}Co_{0.3}Al_{0.1}$ alloy electrode is better than other alloys.

Table 4. Comparison of electrochemical performance of $AB_{3.3}$-type $La_{0.63}Gd_{0.2}Mg_{0.17}Ni_{3.0-x}Co_{0.3}Al_x$ alloys, $La_{0.7}Mg_{0.3}Ni_{2.8}Co_{0.5-x}Al_x$ (x = 0-0.2) alloys [24] and $Mm_{0.83}Mg_{0.17}Ni_{3.1}Al_{0.2}$ alloy [31] at 298 K

Sample	N	C_{max}(mAh g^{-1})	S_{100}(%)
$La_{0.63}Gd_{0.2}Mg_{0.17}Ni_{3.0}Co_{0.3}$	2	371.1	76.2
$La_{0.63}Gd_{0.2}Mg_{0.17}Ni_{2.9}Co_{0.3}Al_{0.1}$	3	363.9	90.4
$La_{0.63}Gd_{0.2}Mg_{0.17}Ni_{2.8}Co_{0.3}Al_{0.2}$	4	340.4	90.6
$La_{0.63}Gd_{0.2}Mg_{0.17}Ni_{2.7}Co_{0.3}Al_{0.3}$	3	321.5	92.6
$La_{0.63}Gd_{0.2}Mg_{0.17}Ni_{2.6}Co_{0.3}Al_{0.4}$	2	257.9	91.8
$La_{0.7}Mg_{0.3}Ni_{2.8}Co_{0.5}$ [24]	2	384.0	55.6
$La_{0.7}Mg_{0.3}Ni_{2.8}Co_{0.4}Al_{0.1}$ [24]	2	367.0	76.5
$La_{0.7}Mg_{0.3}Ni_{2.8}Co_{0.3}Al_{0.2}$ [24]	1	335.0	89.2
$Mm_{0.83}Mg_{0.17}Ni_{3.1}Al_{0.2}$ [31]	3	340.0	93.5

Based on the above analysis, it can be seen that the substitution of Al for Ni is harmful to the charge transfer on the alloy surface. The alloy of x = 0.1 shows the optimal cycling stability and kinetic properties.

4. CONCLUSIONS

1) Partial substitution of Al for Ni is beneficial to the formation of the $CaCu_5$-type phase, which induces the main phase of alloys to shift from Ce_2Ni_7-type (Gd_2Co_7-type) structure to $CaCu_5$-type phase.

2) All of alloy electrodes exhibit a good activation rate, and the discharge capacity is between 257.9 mAh g^{-1} and 371.1 mAh g^{-1} in dependence of the content of Al elements.

3) Function exploration of Al-substituted alloy indicates that the Al-substitution changes to the structure and the pulverization rates of alloys, the resulting superlattice alloys benefit from improved cycling stability and charge retention at the expense of inferior HRD. The x = 0.1 substituted alloy electrode has best the overall electrochemical performances of the alloy electrodes.

ACKNOWLEDGEMENTS

This work was supported by the Nature Science Foundation of Shandong Province (No. ZR2014EMP012, ZR2017QEE014), Doctor Foundation of Binzhou University (No. 2013Y10) and the Science and Technology Development Plan of Bingzhou (No. 2014ZC0216). The authors express sincere thanks to the NSFC (Natural Science Foundation of China, 51404220) for financial support.

References

1. T. Kohno, H. Yoshida, F. Kawashima, T. Inaba, I. Sakai, M. Yamamoto and M. Kanda, *J. Alloys Compd.*, 311 (2000) L5.
2. X.L. Ding, Y.T. Li, F. Fang, D.L. Sun and Q.A. Zhang, *J. Mater. Chem. A*, 5 (2017) 5067.
3. W. Lv and Y. Wu, *J. Alloys Compd.*, 789 (2019) 547.
4. K.T. Moller, T.R. Jensen, E. Akiba and H.-W. Li, *Prog. Nat. Sci.–Mater.*, 27 (2017) 34.
5. Y.T. Li, X.L. Ding, F.L. Wu, F. Fang, Q.A. Zhang and D.L. Sun, *J. Phys. Chem. C*, 120 (2016) 1415.
6. Y.T. Li, L.X. Zhang, Q.A. Zhang, F. Fang, D.L. Sun, K.Z. Li, H. Wang, L.Z. Ouyang and M. Zhu, *J. Phys. Chem. C*, 118 (2014) 23635.
7. Z.J. Gao, Y.C. Luo, R.F. Li, Z. Lin and L. Kang, *J. Power Sources*, 241 (2013) 509.
8. Y.T. Li, F. Fang, X.B. Yu, Q.A. Zhang, L.Z. Ouyang, M. Zhu and D.L. Sun, *Acta Mater.*, 59 (2011) 1829.
9. Z.J. Gao, B. Zhang, Y.C. Luo and H.-W. Li, *J. Taiwan Inst. Chem. Eng.*, 89 (2018) 183.
10. Z.J. Gao, Z.N. Yang, Y.T. Li, A.Q. Deng, Y.C. Luo and H.-W. Li, *Dalton Trans.*, 47 (2018) 16453.
11. Z.J. Gao, L. Kang and Y.C. Luo, *New J. Chem.*, 37 (2013) 1105.
12. Y.T. Li, F. Fang, H.L. Fu, J.M. Qiu, Y. Song, Y.S. Li, D.L. Sun, Q.A. Zhang, L.Z. Ouyang and M. Zhu, *J. Mater. Chem. A*, 1 (2013) 5238.
13. Z.J. Gao, Y.C. Luo, Z. Lin, R.F. Li, J.Y. Wang and L. Kang, *J. Solid State Electrochem.*, 17 (2013) 727.
14. J.H. Zang, Q.A. Zhang, and D.L. Sun, *J. Alloys Compd.*, 771 (2019) 711.
15. L.Z. Ouyang, T.H. Yang, M. Zhu, D. Min, T.Z. Luo, H. Wang, F.M. Xiao and R.H. Tang, *J. Alloys Compd.*, 735 (2018) 98.
16. W. Lv, J.G. Yuan, B. Zhang and Y. Wu, *J. Alloys Compd.*, 730 (2018) 360.
17. M. Nowak, M. Balcerzak and M. Jurczyk, *Int. J. Hydrogen Energy*, 43 (2018) 8897.
18. M. Dymek, M. Nowak, M. Jurczyk and H. Bala, *J. Alloys Compd.*, 780 (2019) 697.
19. F.L. Zhang, Y.C. Luo, A.Q. Deng, Z.H. Tang, L. Kang and J.H. Chen, *Electrochim. Acta*, 52 (2006) 24.
20. K. Aoki, X.-G. Li and T. Masumoto, *Acta Metall.*, 40 (1992) 1717.

21. M.N. Guzik, B.C. Hauback and K. Yvon, *J. Solid State Chem.*, 186 (2012) 9.
22. Y.H. Zhang, P.P. Wang, W.G. Bu, Z.M. Yuan, Y. Qi and S.H. Guo, *RSC Adv.*, 8 (2018) 23353.
23. B. Li, J.D. Li, H.J. Zhao, X.Q. Yu and H.Y. Shao, *Int. J. Hydrogen Energy*, 44 (2019) 6007.
24. K. Young, T. Ouchi, L. Wang and D.F. Wong, *J. Power Sources*, 279 (2015) 172.
25. R.A. Young, The Rietveld Method, Introduction to the Rietveld Method; R.A. Young Eds.; Oxford University Press Inc; New York, 1995, p.1.
26. J. Rodriguez-Carvajal, Abstract of the Satellite Meeting on Powder Diffraction, Congress of IUCr, Toulouse, France, 1990, p. l27.
27. Y. Osumi, H. Suzuki, A. Kato, K. Oguro, S. Kawai and M. Kaneko, *J. Less Comm. Met.*, 89 (1983) 287.
28. K. Young, J. Nei, B. Huang and M.A. Fetcenko, *Int. J. Hydrogen Energy*, 36 (2011) 11146.
29. C.C. Yang, C. C. Wang, M.M. Li and Q. Jiang, *J. Mater. Chem. A*, 5 (2017) 1145.
30. Y.H. Zhang, Z.H. Hou, B.W. Li, H.P. Ren, G.F. Zhang and D.L. Zhao, *J. Alloys Compd.*, 537 (2012) 175.
31. T. Ozaki, M. Kanemoto, T. Kakeya, Y. Kitano, M. Kuzuhara, M. Watada, S. Tanase and T. Sakai, *J. Alloys Compd.*, 446-447 (2007) 620.
32. F. Li, K. Young, T. Ouchi and M.A. Fetcenko, *J. Alloys Compd.*, 471 (2009) 371.
33. F.L. Zhang, Y.C. Luo, J.P. Chen, R.X. Yan and J.H. Chen, *J. Alloys Compd.*, 430 (2007) 302.
34. C. Iwakura, M. Matsuoka, K. Asai and T. Kohno, *J. Power Sources*, 38 (1992) 335.
35. C. Iwakura, T. Oura, H. Inoue and M. Matsuoka, *Electrochim. Acta*, 41 (1996) 117.